The Influence of Fibre Spatial Characteristics on the Flexural Performance of SFRC

T. Bosman

University of Pretoria, Hillcrest, Pretoria, South Africa

+27795277510

tiaan.bosman01@gmail.com

E.P. Kearsley

University of Pretoria, Hillcrest, Pretoria, South Africa

+27839634650

+27123625218

elsabe.kearsley@up.ac.za

ABSTRACT:

Research has shown that the post-peak tensile strength behaviour of Steel Fibre-Reinforced Concrete (SFRC) elements is significantly affected by the distribution of fibres in the section. The pursuit towards the effective and optimal application of SFRC in practice necessitates a thorough understanding of the influence of fibre spatial distribution on composite performance. In this research, the influence of fibre length and volume content on the spatial distribution of fibres was investigated using a photometric image analysis technique. A unique approach was developed that utilizes Voronoi diagrams as the geometric descriptor quantifying fibre spatial distribution. The resulting parameters characterised the sectional dispersion of fibres as well as the degree of clustering and were related to the flexural performance of notched beams tested under three-point loading. The findings of the study highlight the role of fibre length and volume content on the spatial distribution of fibres and it is revealed that the sectional uniformity, inter-batch spatial variability, and degree of clustering are dependent on the number of fibres in the cross section. Furthermore, the results demonstrated the considerable influence of fibre distribution on the flexural performance of SFRC. It was concluded that the variability in flexural strength reduced as the variation in fibre spatial distribution reduced and that extensive clustering had an adverse effect on the effective resistance provided by fibres.

Fibre-reinforced concrete

Image analysis

Voronoi diagram

Fibre distribution

Clustering

INTRODUCTION

The variability associated with Fibre-Reinforced Concrete (FRC) members has repeatedly been cited as a characteristic stunting the structural application of the material [1,2]. The reliability and scattering of test results tend to be the primary concern as these issues have a direct influence on the safety factors to be used for design purposes. The effectiveness of a fibre-reinforced composite element is strongly dependent on the orientation of fibres with respect to the orthogonal direction of the principal tensile stress in the member. Fibre orientation and spatial distribution can be highly variable and in order to assume homogeneous and isotropic material behaviour, large safety factors are required to account for such variability [3]. The demand for material efficiency in construction is perpetually increasing and necessitates greater ingenuity and creativity from the designer. The thorough investigation and characterisation of FRC broadens the practitioner's understanding of the composite and allows effective application of the material to provide enhanced structural performance or reduced construction costs without having to compromise on performance.

Ferrara et al. [4] presented results demonstrating the dependency of toughness properties on the fibre orientation factor derived using image analysis. The authors concluded that by tailoring the casting procedure and the fresh state properties of the mixture, fibres can be effectively orientated along the direction of the tensile stresses. A study by Zhou and Uchida [5] presented results showing that the number of fibres near a fracture surface was linearly dependent on fibre orientation, while the post-cracking flexural strengths exhibited a perfect linear dependence on the effective number of fibres near the crack surface. The anisotropy commonly encountered with sprayed SFRC was investigated by Segura-Castillo et al. [6] by assessing fibre distribution and its influence on the residual tensile strength of sprayed SFRC. The authors found that the spraying process did indeed induce a strong preferential alignment of fibres perpendicular to the spraying direction. The orientation factor in this direction was 3 times greater than the orientation factor in the plane parallel to the spraying direction. The significant anisotropy was also reflected in residual tensile strength results, with the strength of specimen loaded parallel to the spraying direction reaching residual loads 3.5 times greater than those loaded perpendicularly.

Yoo et al. [7] investigated the effect of fibre length and placement method on the flexural behaviour and fibre distribution characteristics of ultra-high-performance FRC. When comparing the results of 19.5 mm and 30 mm fibres, both having an aspect ratio of 100, the authors reported that the flexural response of the 30 mm fibres demonstrated greater scatter than the specimens containing 19.5 mm fibres. Image analyses of the samples also revealed that the 30 mm fibres were less uniformly distributed across a section compared to the 19.5 mm fibre samples. The results from their study suggest that the variation in flexural behaviour of SFRC may be more dependent on the uniformity of fibre distribution than on the magnitude of the fibre orientation factor.

As part of an experimental programme aimed at evaluating the notched 3-Point Bending Test (3PBT) proposed in RILEM TC 162-TDF [8], specimens with varying concrete strength and fibre content were produced and tested by Barr et al. [9]. In a companion study forming part of the programme, Barr et al. [10] assessed the fibre distribution at the cracked section of beam specimens. The results revealed that toughness increased

with the number of fibres across the critical section and that the variation in the total number of fibres increased as fibre content decreased. The authors reported that the variability in strength of the normal strength concrete beams generally decreased as the fibre content increased. It was said that achieving a uniform fibre distribution is more difficult with low fibre contents, which possibly contributed to the observed behaviour.

The concept of defect introduction associated with increasing fibre volume content has long been experimentally observed and findings suggest a competing process of strength enhancement and degradation. Strength degradation is considered to be related to an increase in pores or microcrack density brought about by the addition of fibres. Li [11] speculated that the increase in pores may be due to insufficient compaction and the additional microcracks arise from contacting fibres, unbonded fibre end cracks, or weak fibre-matrix bonding. Naaman and Shah [12] investigated the pull-out of aligned and orientated steel fibres and varied the number of fibres that were simultaneously pulled out of a 625 mm^2 area. A decline in pull-out resistance with increasing fibre density was reported for both orientations. The pull-out resistance of the specimen with the highest fibre density was 86% and 63% of the single fibre resistance, for fibre orientations of 0° and 60°, respectively.

The spatial distribution of aligned Polyvinyl Alcohol (PVA) fibres in extruded cement composites was studied by Akkaya et al. [13] for fibre lengths of 2 mm, 4 mm, and 6 mm. The authors implemented point process statistics to examine the spatial characteristics of the fibre patterns of each fibre length. Functions were derived to describe the degree of fibre clumping, the size of fibre-free regions, and the number of isolated fibres. It was observed that the 2 mm fibres were distributed more uniformly across the cross section than both the 4 mm and 6 mm fibres. The size and number of fibre-free regions increased with increasing fibre length and was found to contribute significantly to the initiation and advance of cracks in the composite.

The effect of fibre dispersion on composite performance was further studied by Akkaya et al. [14] by considering the distribution of 2 mm PVA fibres at multiple crack locations of an individual specimen. The authors observed that cracks formed sequentially depending on the size of the fibre-free areas and degree of fibre clumping. Cross sections with a higher degree of clumping tended to crack before cross sections with more uniformly distributed fibres and the toughness of the composite was found to be dependent on the fibre clumping at the cross section of the first crack. Furthermore, a strong correlation was reported between the cracking load and the size of the fibre-free regions. It was concluded that the fibre-free areas act as flaws in the matrix and reduced the cracking strength of the composite material.

The purpose of the current research was to better understand the influence of fibre spatial characteristics on the flexural performance of SFRC. This was based on the premise that the spatial distribution of fibres has a considerable impact on the variability and performance of composite elements. The primary research objective was formulated to evaluate such a proposition and was concerned with relating flexural strength to the spatial distribution of fibres and equating the variability in flexural strength to the variability in fibre spatial distribution. As part of the primary objective, the influence of fibre clustering on the effective resistance of fibres was assessed.

A secondary research objective was constructed to compliment the primary objective by investigating the influence of fibre length and fibre volume content on the spatial

distribution of fibres. The secondary research objective explored the strong correlation between fibre spatial characteristics and the number of fibres intersecting a plane, which is a function of fibre length and fibre volume content. The statement was approached by implementing Voronoi diagrams to quantify fibre spatial uniformity across a section as well as the variation in fibre dispersion and relating the results to fibre count. Additionally, the relationship between fibre count and the extent of fibre clustering was examined.

The secondary research objective serves to link fibre spatial characteristics to fibre length and volume content, and consequently relate mechanical observations to the measured fibre count. Adopting a structured approach to the issue provided insight into the complex interaction between fibre distribution and the flexural response of composite elements.

EXPERIMENTAL FRAMEWORK

Materials and flexural testing

Two different lengths of hook-ended steel fibres, with similar aspect ratios, were sourced from a local supplier. The fibres were 30 mm and 60 mm in length with wire diameters of 0.5 mm and 0.9 mm, respectively. The nominal tensile strength of both fibres was stated by the supplier as 1100 N/mm^2. The fibre dosages for each fibre length ranged from 40 kg/m^3 to 120 kg/m^3 in intervals of 20 kg/m^3. These dosages roughly translate to fibre volume contents of 0.5, 0.75, 1.0, 1.25, and 1.5 per cent. A total of 10 batches were cast with each batch comprising of 9 flexural beams that were 600 mm long and 150 mm in width and height. The mixture proportions were selected to achieve a target mean compressive strength of 50 MPa after water curing the specimens for 28 days. A conventional mixture with a w/c ratio of 0.5 was designed and each batch was mixed according to the proportions provided in Table 1.

The 3-point bending tests were carried out as recommended by RILEM TC 162-TDF [8] with a slight modification to the length of the loading span. The recommendation specifies that the supports be positioned 500 mm apart, whereas a distance of 450 mm was used for all beams tested in this study. Each specimen was instrumented with 2 Linear Variable Differential Transformers (LVDTs), one on either side of the mid-span, and a clip gauge placed over the centre of the notch underneath the beam. To avoid the effects of extraneous deformation measurements due to local crushing at the supports and loading point, the vertical deflection was measured with respect to the specimen. This was achieved by clamping yoke frames to the specimen at mid-height above the supports and mounting the LVDTs on a horizontal aluminium bar resting on the yokes.

The tests were performed in displacement control such that the average mid-span deflection increased at a constant rate of 0.2 mm/min. The load was applied with the direction of casting perpendicular to the loading direction until a minimum Crack Mouth Opening Distance (CMOD) of 5.5 mm was recorded by the clip gauge. Prior to testing, the dimensions of each beam were measured using a digital vernier caliper. The height of the unnotched section was measured on either side as well as the average width of the specimen at the notch. The depth of the notch was measured at three locations to ensure that the specimen was cut evenly and within the prescribed tolerances.

Image processing

Image analysis refers to the process of objectively assessing an image by extracting specific information and analysing this information in a quantitative manner. Within the scope of this research, the primary data to be extracted was the location of each fibre in an image of a composite beam's cross section. This required the progression of three operations: sample preparation, image acquisition, and feature extraction. The key stages involved in the image processing phase are illustrated in Fig. 9 of the supplementary material.

Preparing the samples involved cutting sections from the tested flexural beams and polishing the surfaces to be used for image analysis. This was a vital step in the process as it may cause significant complications during the subsequent phases if not carried out meticulously. If the samples are not carefully cut, they may require excessive polishing to obtain a smooth and level surface. If the samples are not adequately polished, fibres may not be recognized by the segmentation algorithm or a cluster of several fibres may be erroneously identified as a single entity.

Images of the prepared specimens were captured with a Nikon D7100 digital camera equipped with a Nikon 18 – 140 mm zoom lens. The camera settings and lighting remained constant throughout the process. The lens that was used is known to result in optic distortion of the images and was corrected by post-processing the images in Adobe Lightroom for the specific lens profile.

An image processing algorithm was developed to automatically extract the centroidal coordinates of each fibre from an input image. The procedure was written in MATLAB and can be summarised to consist of the following steps:

1. Top-hat filtering and contrast enhancement;
2. Morphological noise removal;
3. Segmentation by thresholding, and
4. Watershed segmentation using the distance transform.

The purpose of the white top-hat transform in the first step was to correct for possible nonuniform illumination across the image and was implemented in the algorithm as a disk-shaped structuring element. This was followed by adjusting the contrast to saturate the bottom 85% of the pixel intensity values to black and the pixel values above 220 to white. This provided high contrast between the fibres and the surrounding material.

The morphological operations that were implemented removed small noise spots without altering the overall shape of the objects in the image. The morphological techniques are referred to as "opening-by-reconstruction" followed by "closing-by-reconstruction" and a disk-shaped structuring element was used in both processes. Otsu thresholding [15] was then used in step 3 to segment the fibres from the matrix and create a binary image.

The final step was necessary for separating multiple adjacent fibres that were segmented as a single object. This was accomplished by implementing a watershed segmentation algorithm based on the immersion analogy proposed by Vincent and Soille [16]. The underlying idea of the watershed transform intuitively originates from geography. The watershed algorithm identifies "catchment basins" by treating an image as a topographical surface, with low pixel-intensity values representing low elevations

and high pixel values as high elevations. The algorithm involved generating a grayscale distance transform image from a binary image and using the distance transform as an input to the watershed transform algorithm. The distance transform of the binary image provides a metric of separation of points by calculating the distance between each background pixel and the nearest foreground pixel. The resulting transform was a grayscale image with the intensity of pixels in the foreground objects altered to reflect the distance of each point to the closest boundary. The final binary image was then obtained by segmenting the watershed transform grayscale image.

QUANTIFYING FIBRE SPATIAL CHARACTERISTICS

Spatial descriptor: The Voronoi diagram

Once the fibre data were extracted in the form of a binary image, the data required processing to quantitatively characterise the spatial distribution of the fibres. The proposed method involved generating a Voronoi diagram to objectively tesselate the cross section into discrete regions corresponding to the location of each fibre.

A Voronoi diagram is constructed from a given set of "sites" to form a collection of regions that divide up the plane. Each site corresponds to one of the regions and all points within a region are closer to the corresponding generator site than any other site. Where a point is equidistant to two sites (β in Fig. 1), there is a boundary line that delineates two regions. Boundary lines intersect to form vertices, which are points that are equidistant to three or more generator sites [17]. These concepts are illustrated in Fig. 1.

The distance between a vertex and the nearest fibre(s), indicated in Fig. 1 as α, is the measure that was ultimately selected to define fibre spatial distribution. The distance represents the radius of the largest circle bordering three or more fibres that does not contain any fibres. The area of the region attributed to each fibre is an alternative measure that could also have sufficed; however, such a measure was expected to reflect fibre clustering less effectively. The size of Voronoi regions do not adequately reflect the spacing between fibres because a fibre is not necessarily located near the centre of its regions nor are the Voronoi regions regularly shaped. Therefore, clusters of fibres may not be identified due to the misinterpretation of the size of their regions.

Fibre dispersion

Fibre dispersion is a measure of the uniformity or homogeneity of fibre spatial distribution in a cross section. The statistical variance of the Voronoi spacing data is equivalent to the spread of the distribution and was therefore used to quantify the dispersion of fibres in the composite. As part of the primary research objective, spatial distribution was described by fibre dispersion and was expected to correlate with the flexural strength of the composite beams. Based on such a proposition, the variation in dispersion should demonstrate a positive correlation with the variation in flexural strength. The variation in fibre dispersion was defined as the sample standard deviation of a batch of fibre dispersion results.

Degree of clustering

Assessing whether a point pattern exhibits clustering required that an objective control criterion be defined. The condition of Complete Spatial Randomness (CSR) was selected for this purpose and was modelled as a Poisson process. A Poisson process represents a fibre pattern that is completely random and has no systematic tendencies for fibres to avoid one another or form clusters. It is well known that fibres are not spatially randomly distributed and that factors such as the presence of boundaries, fresh-state properties, and casting procedures certainly affect the distribution of fibres in a plane. The condition of CSR is therefore only used to assess the extent that the fibre pattern deviates from a Poisson point pattern.

The process of quantifying the degree of clustering involved fitting a distribution function to the Voronoi spacing results, evaluating the deviation from a CSR point pattern of the same point density, and accounting for the influence of fibre proximity on the effective fibre resistance.

A Nakagami type distribution was selected as the most suitable fit to the Voronoi results of the CSR patterns as well as the fibre patterns. The distribution is related to the Gamma distribution and was originally introduced by Nakagami [18] to model right-skewed positive data sets. The Nakagami Probability Density Function (PDF) is described by a shape parameter, affecting the shape of the distribution, and a scale parameter, controlling the spread of the distribution. Therefore, fitting a Nakagami type distribution to several generated CSR patterns provided shape factors that are approximately equal, regardless of the point density, and scale parameters that decreased as the point density of the pattern increased.

The Voronoi diagrams and associated probability distributions for simulated patterns exhibiting clustering, CSR, and regularity are shown in Fig. 2. Although the patterns are evidently dissimilar, the mean Voronoi fibre spacing of each pattern is approximately equal. However, the distinct spatial distribution of each pattern is well reflected by the variance in Voronoi spacing (dispersion) and the shape factors obtained from the fitted Nakagami distribution functions.

The properties of a Nakagami type distribution constitute that a low shape factor is generally associated with a clustered pattern. However, depending on the variance of the random pattern shape factor distribution, a low shape factor may still be within the probable range of shape factors. Considering the distributions shown in Fig. 3, for a fibre count of 100, a shape factor equal to 1.5 is within the range of values obtained from a random pattern and it is therefore statistically probable that the fibres are randomly distributed. Whereas for a fibre count of 1000, it is highly improbable that a shape factor of 1.5 will result from a random pattern and that the fibres are likely exhibiting a more clustered distribution. This implies that the shape factor alone does not provide a sufficient indication of clustering and that the distribution of possible CSR shape factors must first be considered.

Probability distributions of Nakagami shape factors were obtained from 2500 CSR point simulations, of various point densities, and employed to assess the degree of clustering of fibre patterns of similar point densities. The CSR shape factor distributions were similar to those depicted in Fig. 3.

Assuming that the shape factor for a random point process is distributed according to a lognormal distribution, the probability that a given shape factor forms part of such a distribution can be determined and used to assess whether the fibre distribution is characteristic of a random pattern or a clustered pattern. This involved the following sequence of steps:

1. The lognormal distribution for the shape factors of a specified fibre density was obtained from several simulations of CSR point patterns (Fig. 3);
2. The lognormally distributed variable X was transformed to the normally distributed variable W using the transformation $\ln(X) = W$, and
3. The mean θ and variance ω^2 of the transformed data was then used to calculate the standard normal random variable as $z = \frac{\ln(x)-\theta}{\omega}$.

If it can be said that the standard normal random variable, z, provides a measure of clusteredness with respect to a random point process of the same point density, then the relative degree of clustering with respect to the number of fibres affected can be defined as:

$$CL = \left| z \cdot N_f \right| \quad (1)$$

where: CL is the relative degree of clustering; z is the calculated standard normal random variable; and N_f is the number of fibres intersecting the cross section.

The N_f term is included in Equation 1 to account for the influence of fibre proximity on the effective resistance provided by fibres. The degree of fibre clustering may therefore be described as the extent to which the shape parameter of a fibre pattern deviates from the distribution of shape parameters obtained from CSR simulations of the same point density. All calculated values of z were negative and therefore taking the absolute value of the term, as in Equation 1, has no consequence and merely transforms the data to the more familiar domain of natural numbers.

RESULTS AND DISCUSSION

Flexural testing results

RILEM TC 162-TDF [8] provides two approaches for deriving flexural strength parameters from 3PBT data. The first approach involves calculating the equivalent flexural tensile strengths and the second approach the residual flexural tensile strengths. In both cases it is assumed that the stress distribution in the cross section is linear elastic. It has been pointed out by some authors [19,20] that although the residual flexural strength parameters have the advantage of a more simplified derivation, they are more susceptible to local irregularities in the load-CMOD curve and may provide results that show a larger amount of scatter than the equivalent strength parameters. The equivalent flexural tensile strength parameter $f_{eq,2}$ provides a measure of the energy absorption capacity provided by the fibre reinforcement mechanisms at low midspan deflections (<0.70 mm) and was selected as the flexural strength descriptor in this research.

Fig. 4 shows boxplots of the $f_{eq,2}$ results obtained from the 30 mm and 60 mm fibre mixtures. The trends in the results indicate that a lower variation in flexural strength

was generally demonstrated by the mixtures containing 30 mm fibres compared to the 60 mm fibre mixtures. A distinct increase in flexural strength with increasing fibre content is evident in Fig. 4, with the 60 mm fibre mixtures achieving the greatest flexural strengths at fibre contents above 60 kg/m^3. Furthermore, the improvement in flexural strength of the 30 mm fibres was inconsequential for fibre dosages of 80 kg/m^3 and greater, whereas the 60 mm fibre results exhibited a more substantial improvement in average flexural strength as the dosage of 60 mm fibres was increased. The mean Stress-CMOD curves for the various fibre dosages are shown in Fig. 10 contained in the supplementary material.

Image analysis results

The secondary research objective was concerned with the influence of fibre length and volume content on the spatial characteristics of fibres. The matter was assessed by utilizing the Voronoi data obtained from image analyses, deriving the proposed spatial parameters, and relating the results to fibre count.

The distance between a vertex and the nearest fibre(s) was selected as the geometric descriptor used to quantify the spatial distribution of fibres. The descriptor is designated as the dimension α in Fig. 1. The parameter provides an indication of the average spacing between a group of three or more fibres and can therefore be used to determine an overall frequency distribution describing the proximity of fibres towards one another.

The histograms and Nakagami fits of the various batches are shown in Fig. 11 of the supplementary material. The figure illustrates that the data can be suitably described by a Nakagami type distribution and that the fibre count has a distinct influence on the spatial distribution of fibres.

To investigate the presence of preferential fibre alignment due to wall-effects as well as the general homogeneity of fibre distribution in a cross section, contour plots of selected batches were constructed to visually illustrate fibre density as presented in Fig. 11. The density plots show limited indication of an increase in fibre concentration in the vicinity of boundaries due to preferential fibre alignment caused by wall-effects; instead a decrease in the fibre density was observed. Although several researchers [21-23,1] have reported that fibre concentration tends to marginally increase as a boundary is approached, the contour plots in Fig. 11 demonstrate that fibres were homogenously distributed, and that casting procedures and fresh-state mixture properties did not have a substantial effect on the distribution of fibres.

As part of the secondary research statement, the relationship between fibre dispersion and fibre count was evaluated. It was expected that the relative spatial uniformity of fibres improves as the number of fibres in a section increases. Fibre dispersion was proposed as a measure to quantify the spatial uniformity of fibres in a cross section and was defined as the statistical variance of Voronoi spacing. The correlation between dispersion and fibre count is demonstrated in Fig. 5a.

Furthermore, it was anticipated that the variation in fibre dispersion will reduce as the number of fibres intersecting the section increases. Variation in dispersion was defined as the sample standard deviation of the dispersion of a batch of specimens and is plotted against the average fibre count in Fig. 5b. The trend in Fig. 5b supports the

notion that the variability in spatial distribution reduces as the number of fibres intersecting the plane increases.

The relationship between fibre clustering and fibre length and dosage was investigated by relating a measure of fibre clusteredness, such as z, to the number of fibres intersecting a cross section. Extensive fibre clustering was expected to correspond to high fibre counts and therefore short fibre lengths and high fibre dosages. Plotting the standard normal random variable, z, against the number of fibres produced the trend shown in Fig. 5c. The figure substantiates the proposition that fibre clustering is positively correlated to the number of fibres in a section.

Relating composite performance and fibre distribution

In investigating the primary research objective, it was expected that the flexural strength of a composite member will increase as the uniformity of fibre spatial distribution increases. This proposition was based on the premise that fibres act as defects in the matrix. Therefore, members with poorly dispersed fibres contain regions with low fibre concentrations, which require less energy for cracks to initiate and easily propagate through the unsupported matrix. Conversely, a composite section with uniformly dispersed fibres minimises the size of such regions, increasing the probability of bridging a crack, and consequently maximising the reinforcement efficiency.

The relationship between dispersion and equivalent flexural strength, $f_{eq,2}$, is illustrated in Fig. 6a and Fig. 6b for 30 mm and 60 mm fibres, respectively. The exponential fits applied to the data in Fig. 6 provide a qualitative indication of the strong correlation between flexural strength and dispersion and substantiate the notion that a more uniform fibre distribution enhances the flexural strength of a composite element.

Considering the outcome of this proposition, it is intuitive and logical to deduce that the variability in flexural strength will increase as the variability in fibre dispersion increases. The Coefficient of Variation (CoV) was selected as a measure to quantify the variability in equivalent flexural strength of a batch of specimens. The CoV of $f_{eq,2}$ is plotted against the sample standard deviation of dispersion in Fig. 7. The power function fitted to the results only serves to demonstrate the positive correlation between the variability in flexural strength and – fibre dispersion and no definitive conclusions regarding the nature of the relationship could be reached based on the available data.

In order to evaluate whether flexural strength is influenced by fibre clustering, a normalised measure of strength is required to account for the number of fibres intersecting the cross section. To obtain such a measure, it was firstly required that the number of 60 mm fibres be converted to an equivalent number of 30 mm fibres. Linear regression was performed on the data by plotting the average number of 30 mm fibres against the average 60 mm fibre count and yielded the relation $N_{f,30} = 2.882 \cdot N_{f,60}$. The equivalent number of 30 mm fibres was then determined by multiplying the fibre count of the 60 mm batches with the factor of 2.882. The equivalent fibre resistance was then calculated as follows:

$$\tau_{eq} = \frac{f_{eq,2}}{N_{f,30}} \cdot 1000 \qquad (2)$$

where: τ_{eq} is the equivalent fibre resistance with units kPa/fibre; and $N_{f,30}$ is the equivalent number of 30 mm fibres.

The relationship between equivalent fibre resistance and the degree of clustering is demonstrated in Fig. 8. The trend exhibited by the data in Fig. 8 suggests that the equivalent fibre resistance decreases as the degree of clustering increases. High fibre counts are considered to cause microstructural inhomogeneity, which deteriorates the mechanical properties of the composite, and the increased fibre interactions lead to a less effective stress transferring mechanism. As expected, the 60 mm fibre results showed limited dependency to the degree of clustering and the negative effects of fibre clustering were only apparent for the 30 mm fibre mixtures at dosages of 80 kg/m^3 and higher. This behaviour can be explained by the mechanisms presumed to contribute to the degree of clustering. An increase in the degree of clustering corresponds to an increase in the number of fibres in a cluster as well as the spacing of fibres in a cluster. This is an unlikely combination for low fibre counts and a more likely combination for high fibre counts as exhibited by the results.

A large degree of scatter was demonstrated by the specimen results, with the trend of variation suggesting that the scatter in 60 mm fibre results was more pronounced than the 30 mm fibre results. This observation is in agreement with the findings presented in the preceding section and supports the proposition that the variability of fibre dispersion reduces as fibre count increases.

CONCLUSSIONS

The study set out to investigate the influence of fibre spatial characteristics on the flexural performance of steel fibre-reinforced concrete. A structured approach to the issue was adopted by constructing primary and secondary research objectives to systematically explore the problem statement. The primary research objective was concerned with relating fibre spatial characteristics to the flexural performance of specimens and the secondary objective was formulated to investigate the influence of fibre length and fibre volume content on the spatial distribution of fibres. The experimental results presented in this research demonstrated the considerable impact of fibre spatial characteristics on the flexural performance of SFRC. The unique analysis techniques provided a new perspective on the mechanisms dictating fibre spatial distribution and gave insight into the interaction between fibre distribution and composite performance.

It was proposed that Voronoi diagrams, generated from fibre locations, be utilized to derive a geometric descriptor that characterised fibre spatial distribution. The method proved to objectively tesselate the cross section and adequately represent the spatial arrangement of fibres. Dispersion was defined as the variance of Voronoi spacing and represented the uniformity of fibre distribution. It was found that dispersion as well as variation in dispersion demonstrated a strong correlation with fibre count and decreased as the number of fibres increased. Lower fibre dispersion and inter-batch variation was observed for the 30 mm fibres compared to the 60 mm fibres due to the larger number of 30 mm fibres intersecting a section at the same volume content. A distinct correlation between fibre clustering and the number of fibres in a section was observed, with the degree of clustering increasing as the fibre count increased. Consequently, the degree of clustering was greater for the specimens containing 30 mm

fibres than for the 60 mm fibre specimens due to the greater number of 30 mm fibres intersecting a given plane.

It was shown that the equivalent flexural tensile strength is influenced by the spatial distribution of fibres and increased as the dispersion of the fibre under consideration decreased. A positive correlation was observed between the CoV of equivalent flexural strength and the standard deviation of fibre dispersion. The variation in flexural response and fibre dispersion was lower for the 30 mm fibres than the 60 mm fibres, and the trend suggested that the variation reduced as fibre count increased. The influence of fibre clustering on the resistance of fibres was investigated and the results revealed that the equivalent fibre resistance decreased as the degree of clustering increased. A notable amount of scatter was observed at low degrees of clustering, which was attributed to the high variation in flexural strength also encountered at low fibre counts. The 60 mm fibres showed limited decrease in fibre resistance and the effects of fibre clustering only become apparent at 30 mm fibre dosages of 80 kg/m^3 and greater.

Although expressions were not formulated for estimating fibre spatial distribution and the influence of fibre distribution on flexural response, this work serves as a preliminary investigation whereupon future research can elaborate. A thorough understanding of the influence of fibre spatial distribution on composite performance is the first step in incorporating fibre distribution into material and structural design procedures and aids the pursuit towards effective, optimal, and efficient implementation of FRC in practice.

References

1. Laranjeira F, Grünewald S, Walraven J, Blom C, Molins C, Aguado A (2011) Characterization of the orientation profile of steel fiber reinforced concrete. Mater Struct 44 (6):1093-1111

2. Parmentier B, Vandewalle L, Van Rickstal F (2008) Evaluation of the scatter of the postpeak behaviour of fibre reinforced concrete in bending: A step towards reliability. In: Gettu R (ed) BEFIB 2008: 7th RILEM International Symposium on Fibre Reinforced Concrete. RILEM Publications SARL, pp 133-143

3. Di Prisco M, Plizzari G, Vandewalle L (2009) Fibre reinforced concrete: new design perspectives. Mater Struct 42 (9):1261-1281

4. Ferrara L, Ozyurt N, Di Prisco M (2011) High mechanical performance of fibre reinforced cementitious composites: the role of “casting-flow induced” fibre orientation. Mater Struct 44 (1):109-128

5. Zhou B, Uchida Y (2017) Relationship between fiber orientation/distribution and post-cracking behaviour in ultra-high-performance fiber-reinforced concrete (UHPFRC). Cem Concr Compos 83:66-75

6. Segura-Castillo L, Cavalaro SHP, Goodier C, Aguado A, Austin S (2018) Fibre distribution and tensile response anisotropy in sprayed fibre reinforced concrete. Mater Struct 51 (1):29

7. Yoo D-Y, Kang S-T, Yoon Y-S (2014) Effect of fiber length and placement method on flexural behavior, tension-softening curve, and fiber distribution characteristics of UHPFRC. Constr Build Mater 64:67-81

8. RILEM TC 162-TDF (2002) Recommendations of RILEM TC 162-TDF: Test and design methods for steel fibre reinforced concrete: bending test. Mater Struct 35 (9):579-582

9. Barr B, Lee M, de Place Hansen EJ, Dupont D, Erdem E, Schaerlaekens S, Schnütgen B, Stang H, Vandewalle L (2003) Round-robin analysis of the RILEM TC 162-TDF beam-bending test: part 1—test method evaluation. Mater Struct 36 (9):609-620

10. Barr B, Lee M, de Place Hansen EJ, Dupont D, Erdem E, Schaerlaekens S, Schnütgen B, Stang H, Vandewalle L (2003) Round-robin analysis of the RILEM TC 162-TDF beam-bending test: Part 3—Fibre distribution. Mater Struct 36 (9):631-635

11. Li VC (1992) A simplified micromechanical model of compressive strength of fiber-reinforced cementitious composites. Cem Concr Compos 14 (2):131-141

12. Naaman AE, Shah SP (1976) Pull-out mechanism in steel fiber-reinforced concrete. ASCE J Struct Div 102 (8):1537-1548

13. Akkaya Y, Peled A, Shah S (2000) Parameters related to fiber length and processing in cementitious composites. Mater Struct 33 (8):515-524

14. Akkaya Y, Shah SP, Ankenman B (2001) Effect of fiber dispersion on multiple cracking of cement composites. J Eng Mech 127 (4):311-316

15. Otsu N (1979) A threshold selection method from gray-level histograms. IEEE transactions on systems, man, and cybernetics 9 (1):62-66

16. Vincent L, Soille P (1991) Watersheds in digital spaces: an efficient algorithm based on immersion simulations. IEEE Transactions on Pattern Analysis & Machine Intelligence (6):583-598

17. De Berg M (2008) Computational geometry: algorithms and applications. 3rd edn. Springer, Berlin

18. Nakagami M (1960) The m-distribution—A general formula of intensity distribution of rapid fading. In: Hoffman WG (ed) Statistical methods in radio wave propagation. Permagon Press, Oxford, UK, pp 3-36

19. Barros JA, Cunha VM, Ribeiro AF, Antunes J (2005) Post-cracking behaviour of steel fibre reinforced concrete. Mater Struct 38 (1):47-56

20. Nayar SK, Gettu R (2014) Characterisation of the toughness of fibre reinforced concrete–revisited in the Indian context. Indian Concr J 88 (2):8-23

21. Alberti M, Enfedaque A, Gálvez J (2017) On the prediction of the orientation factor and fibre distribution of steel and macro-synthetic fibres for fibre-reinforced concrete. Cem Concr Compos 77:29-48

22. Dupont D, Vandewalle L (2005) Distribution of steel fibres in rectangular sections. Cem Concr Compos 27 (3):391-398

23. Kooiman AG (2000) Modelling steel fibre reinforced concrete for structural design. PhD, Delft University of Technology, Delft, Netherlands

Table 1. Mixture components by mass (kg/m^3)

Component	Type	Relative Density	Batch fibre content (kg/m^3)				
			40	60	80	100	120
Cement	CEM Ⅰ52.5N	3.14	460	460	460	460	460
Water	Tap water	1.00	230	230	230	230	230
Coarse aggregate	9.5 mm Dolomite	2.85	883	876	868	861	854
Fine aggregate	4.75 mm Dolomite	2.85	880	880	880	880	880
Steel fibre	Hook-ended	7.87	40	60	80	100	120
Theoretical density	-	-	2493	2506	2518	2531	2544

Figure 1. Components and characteristics of a Voronoi diagram

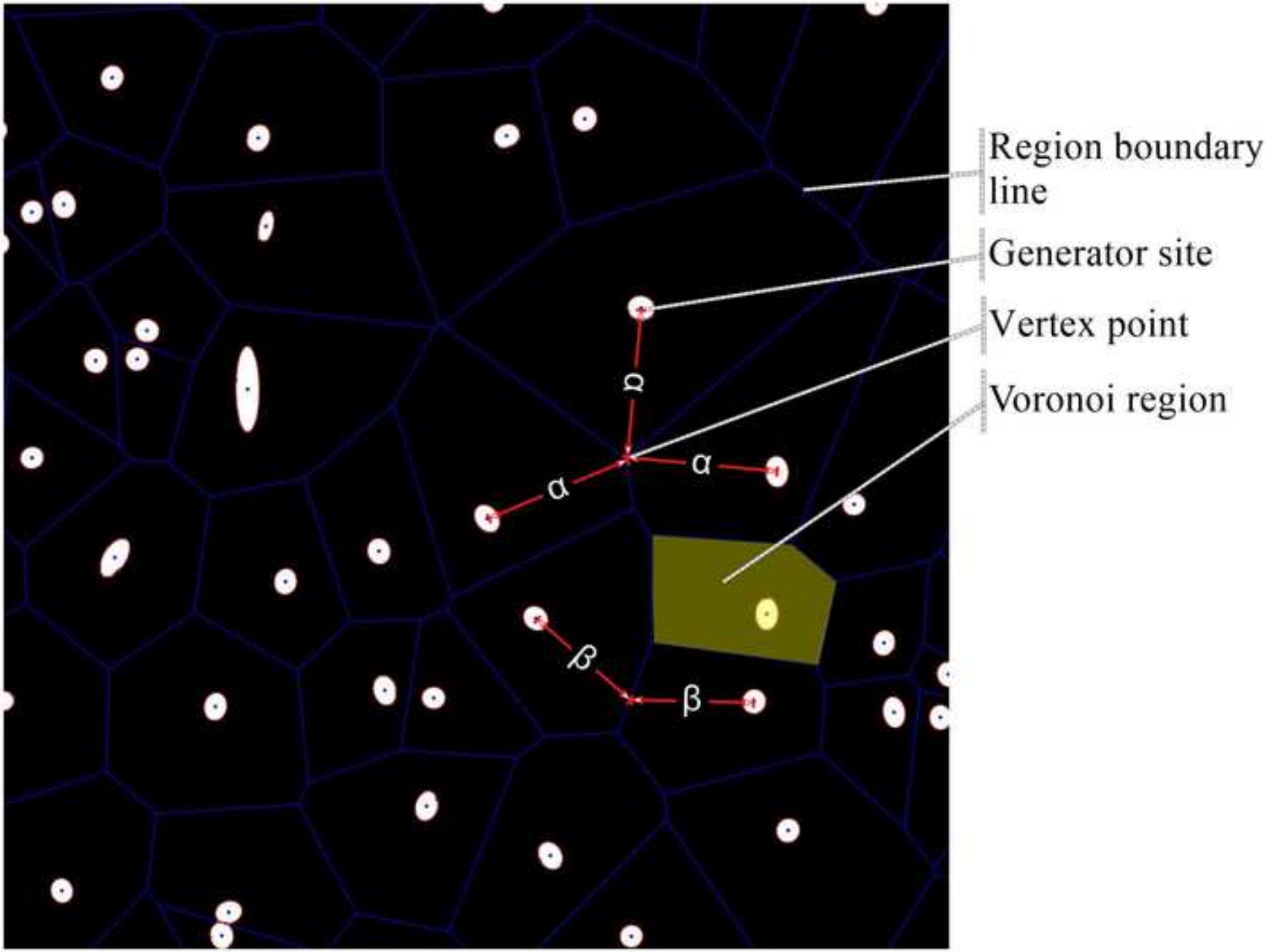

Figure 2. PDFs and Voronoi diagrams of simulated patterns demonstrating clustering, CSR, and regularity

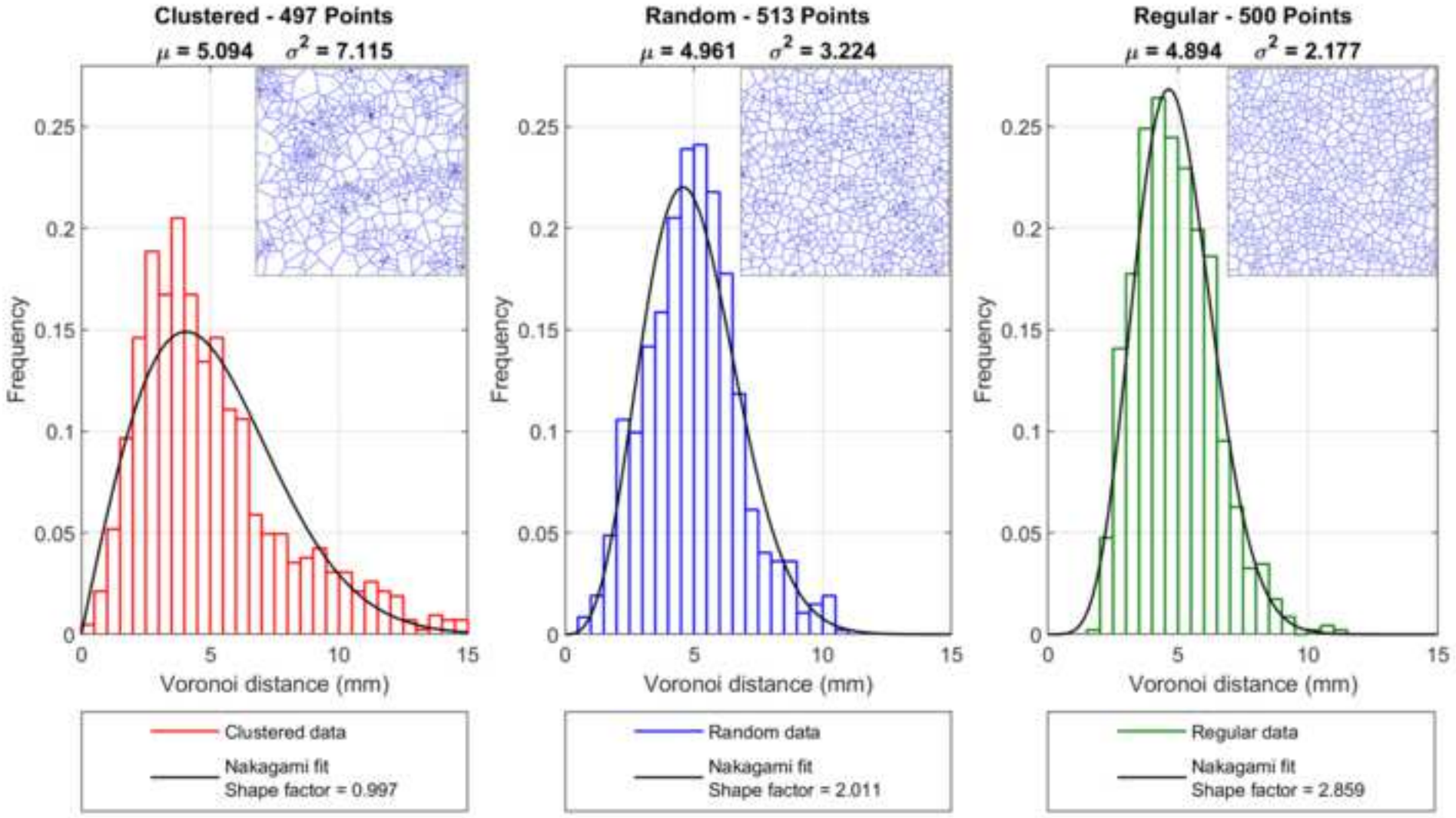

Figure 3. Nakagami shape factor distribution of 2500 random point simulations with 100 and 1000 points

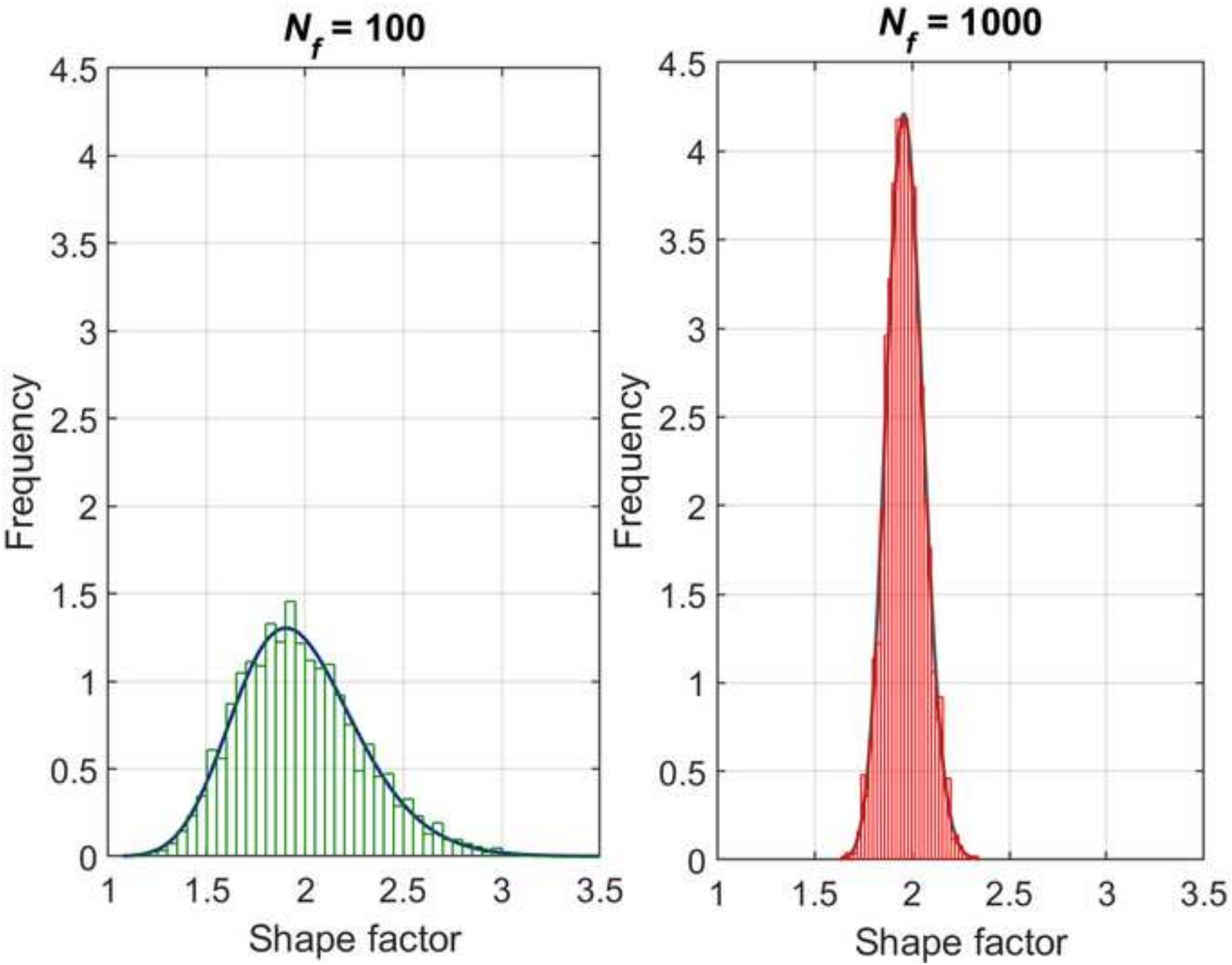

Figure 4. Boxplot of $f_{eq,2}$ results for (a) 30 mm fibres, (b) 60 mm fibres

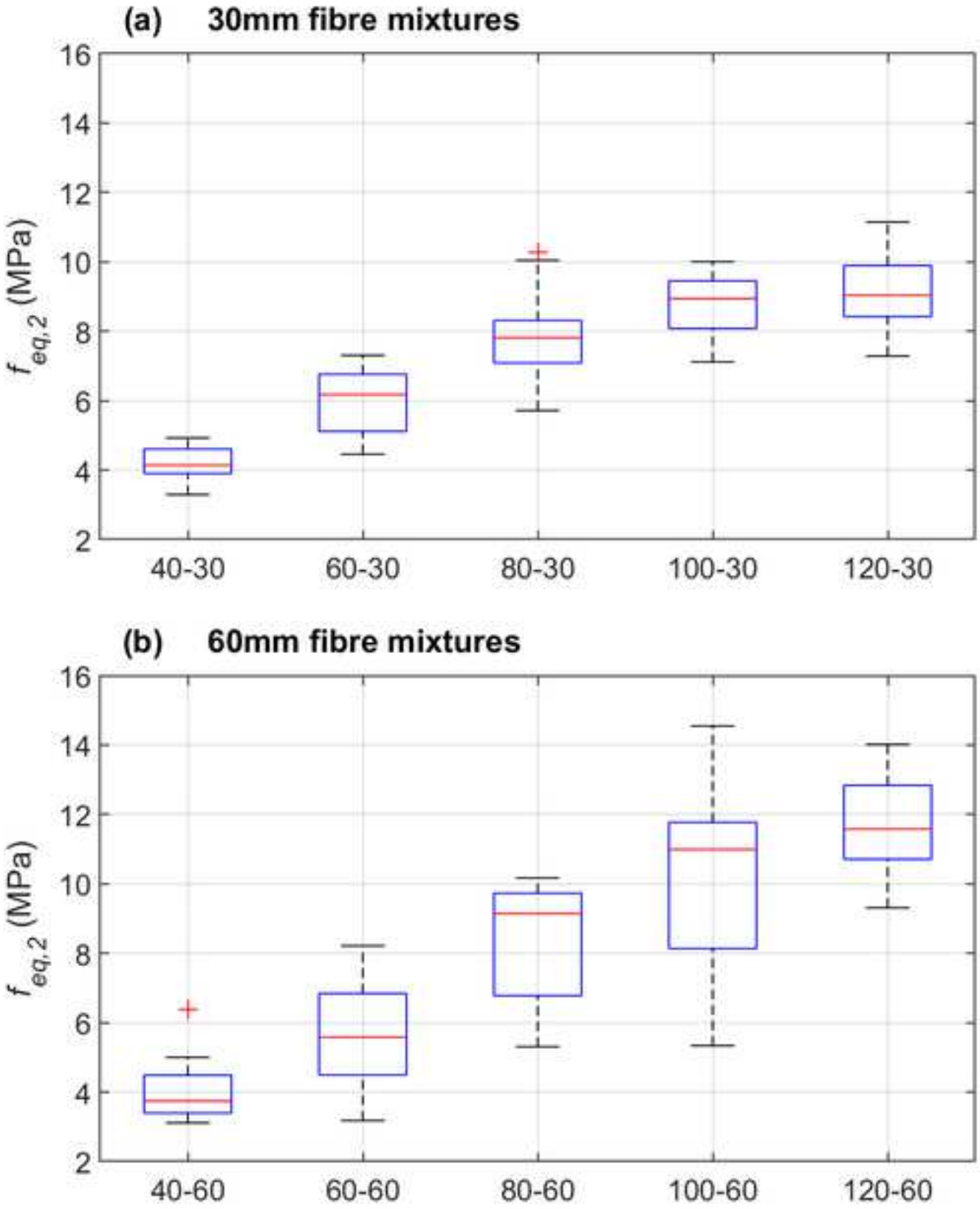

Figure 5. Relating fibre count to (a) dispersion, (b) variation in dispersion, (c) fibre clustering

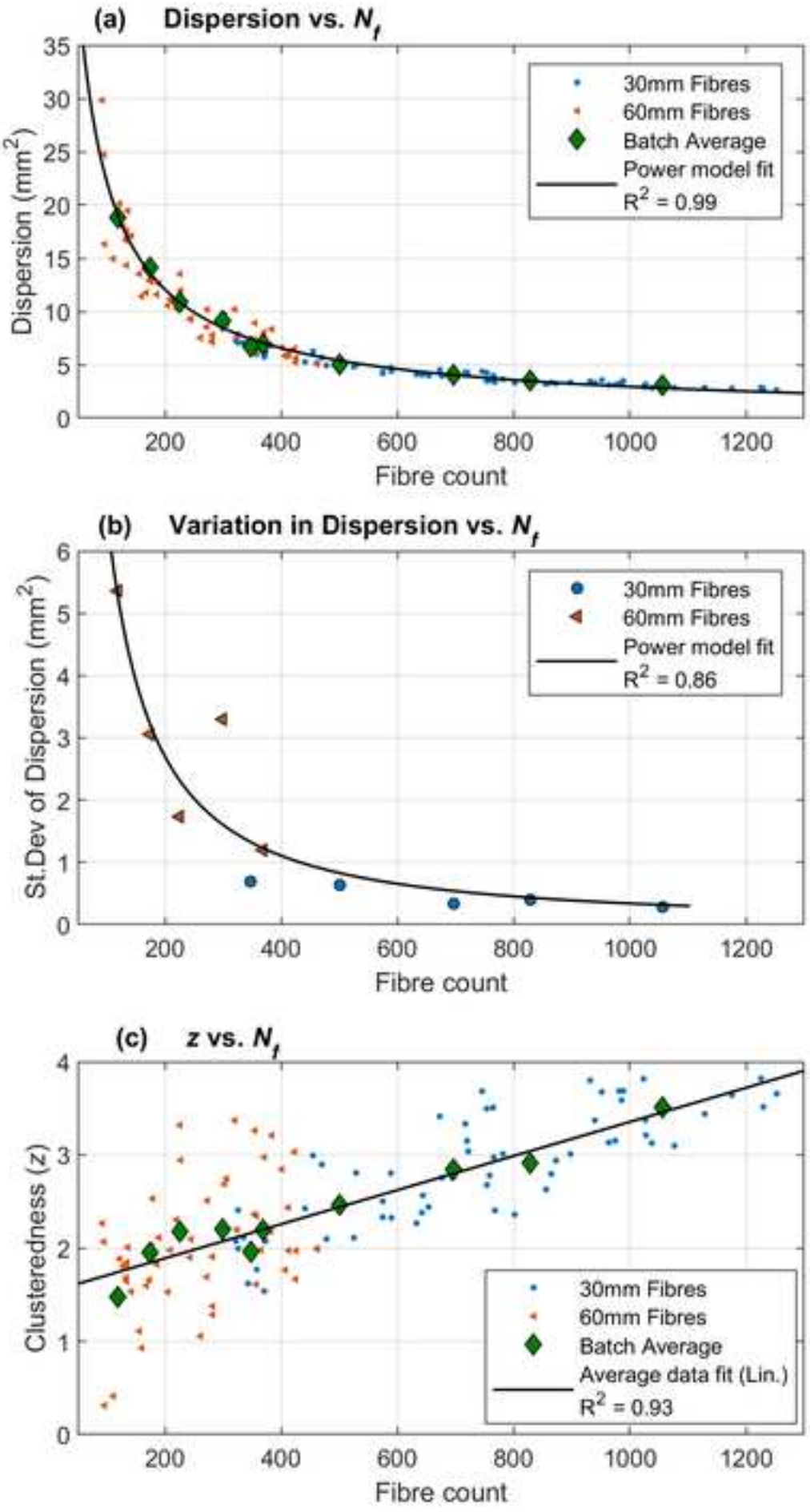

Figure 6. Relationship between dispersion and $f_{eq,2}$ for (a) 30 mm fibres, (b) 60 mm fibres

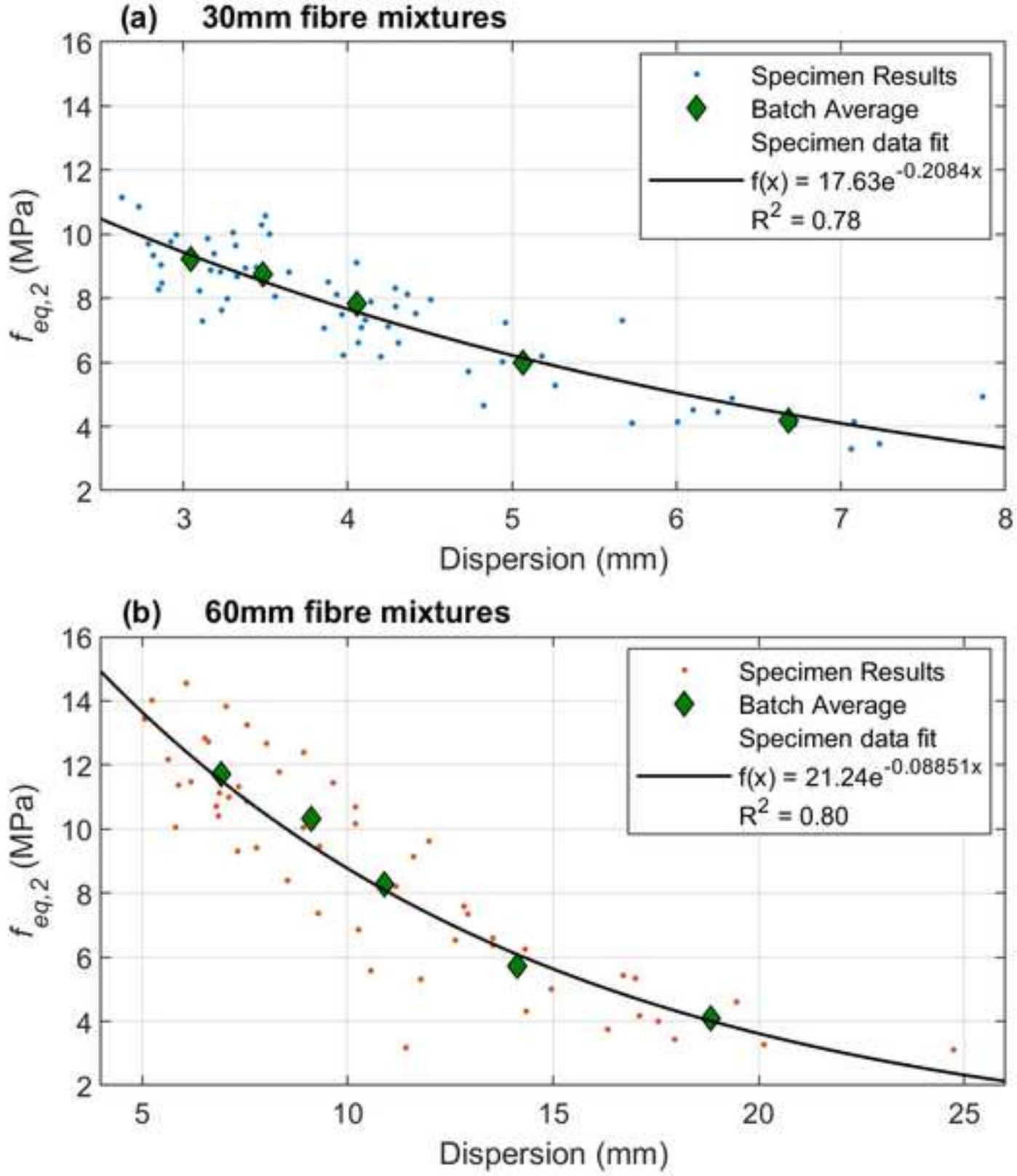

Figure 7. Correlation between the variability in flexural strength and – fibre dispersion

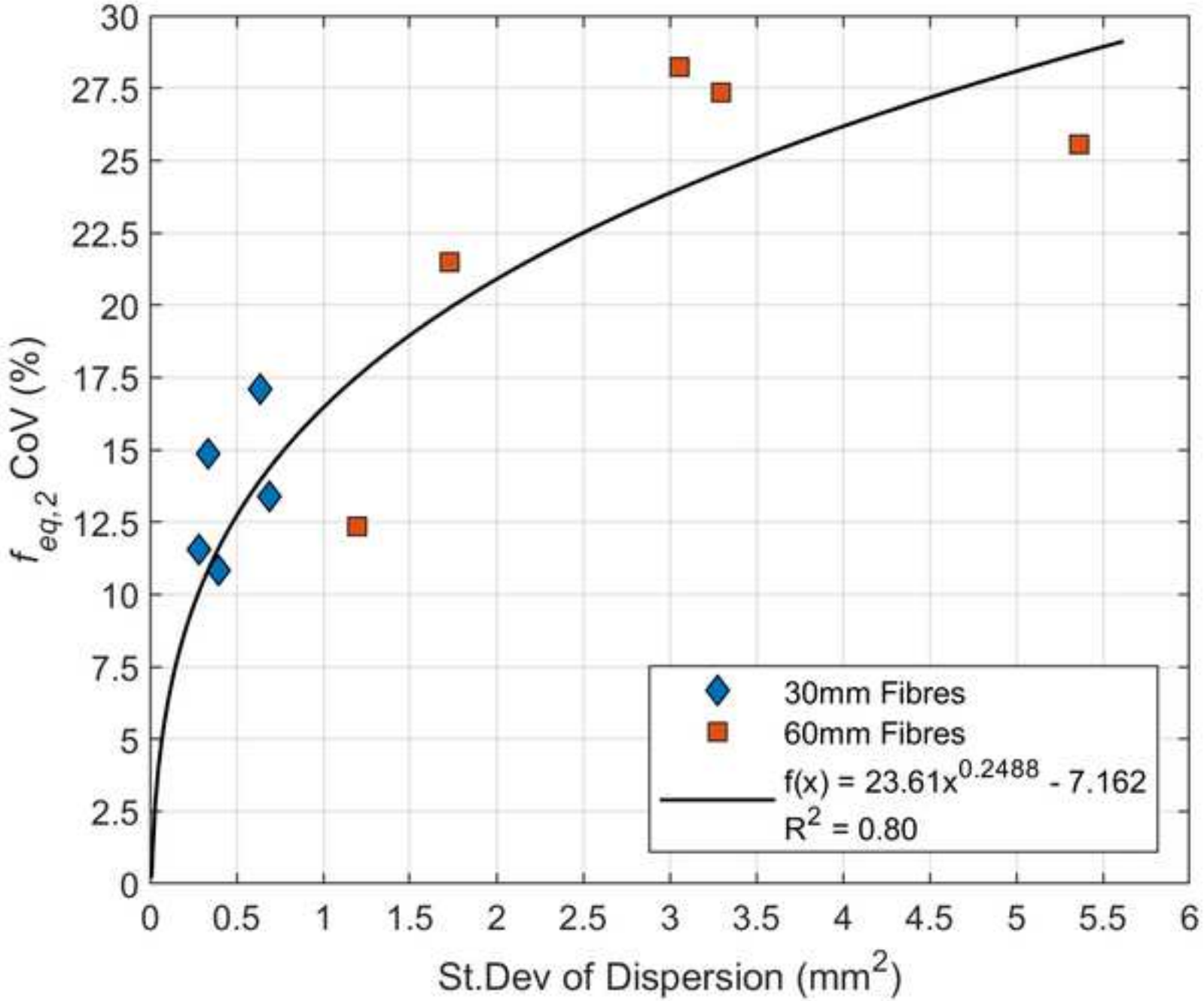

Figure 8. Relationship between equivalent fibre resistance and degree of clustering

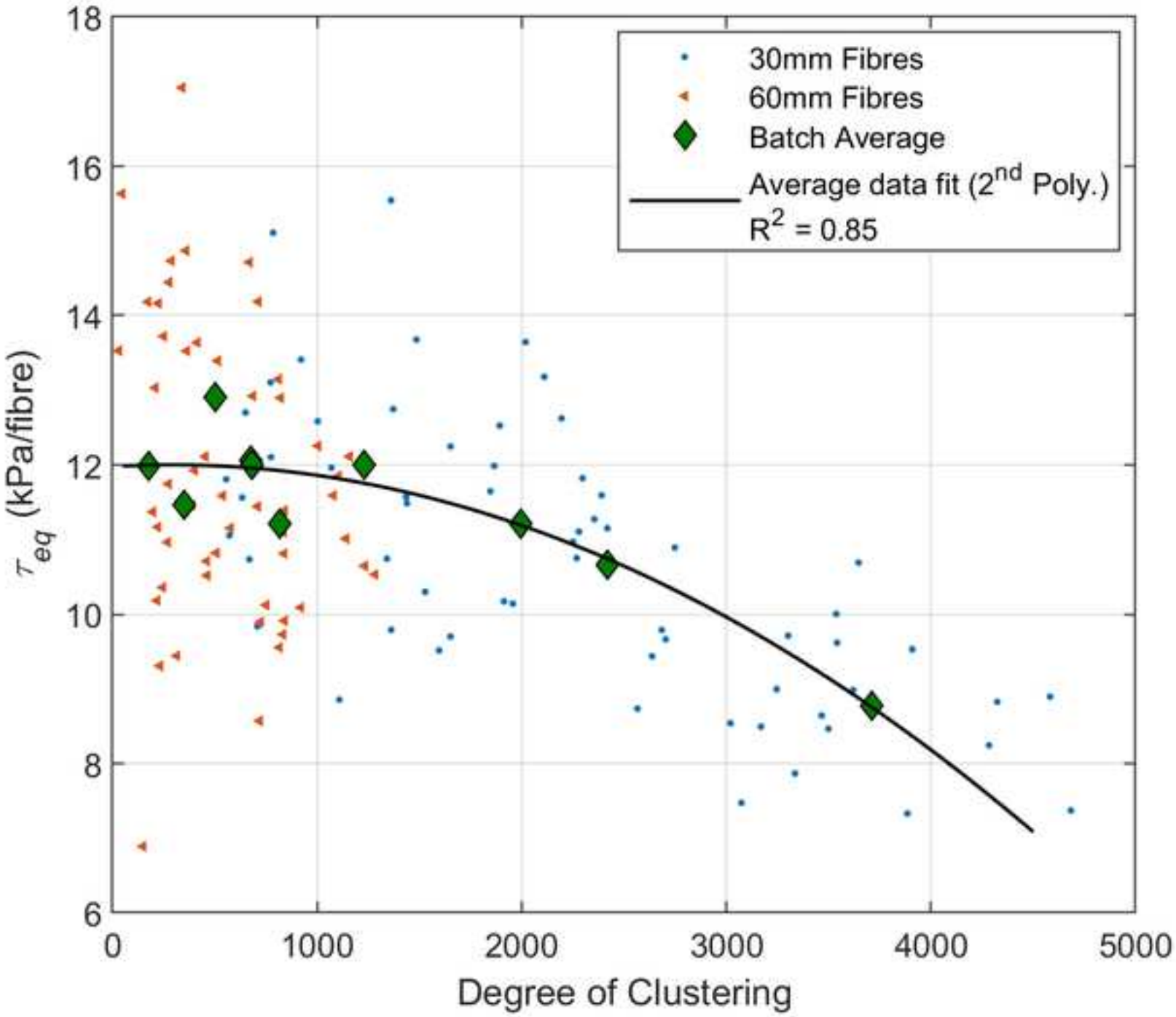

Supplementary Figures

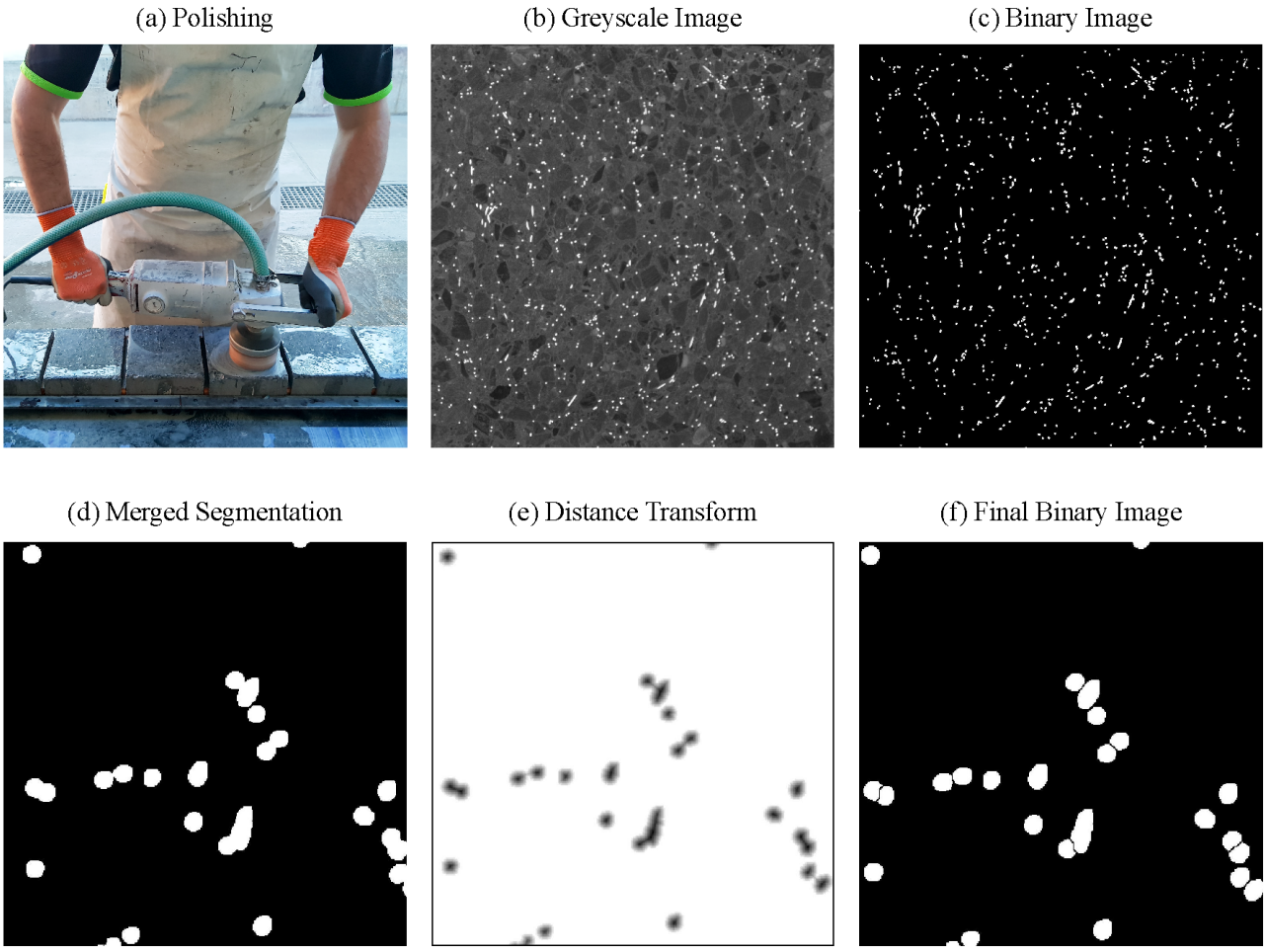

Figure 9. Key stages in the image processing phase

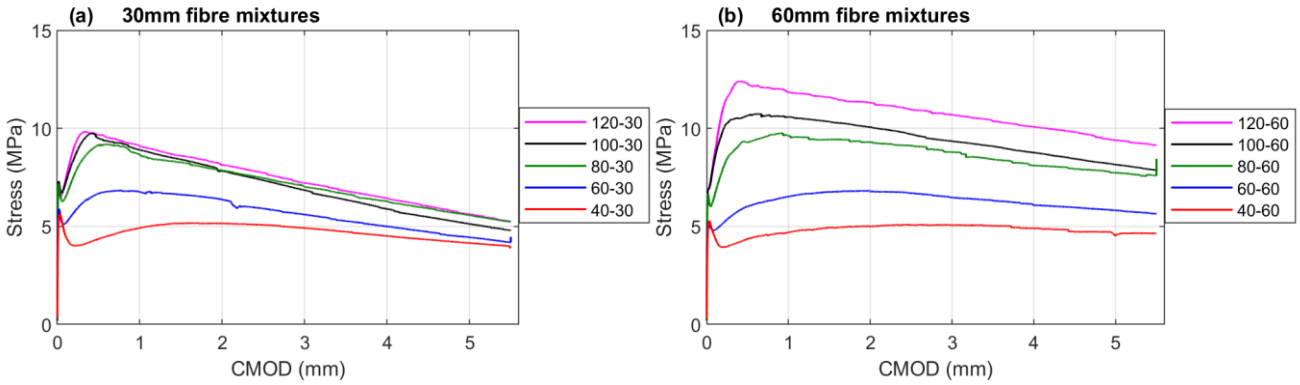

Figure 10. Average flexural response for various dosages of (a) 30 mm fibres, (b) 60 mm fibres

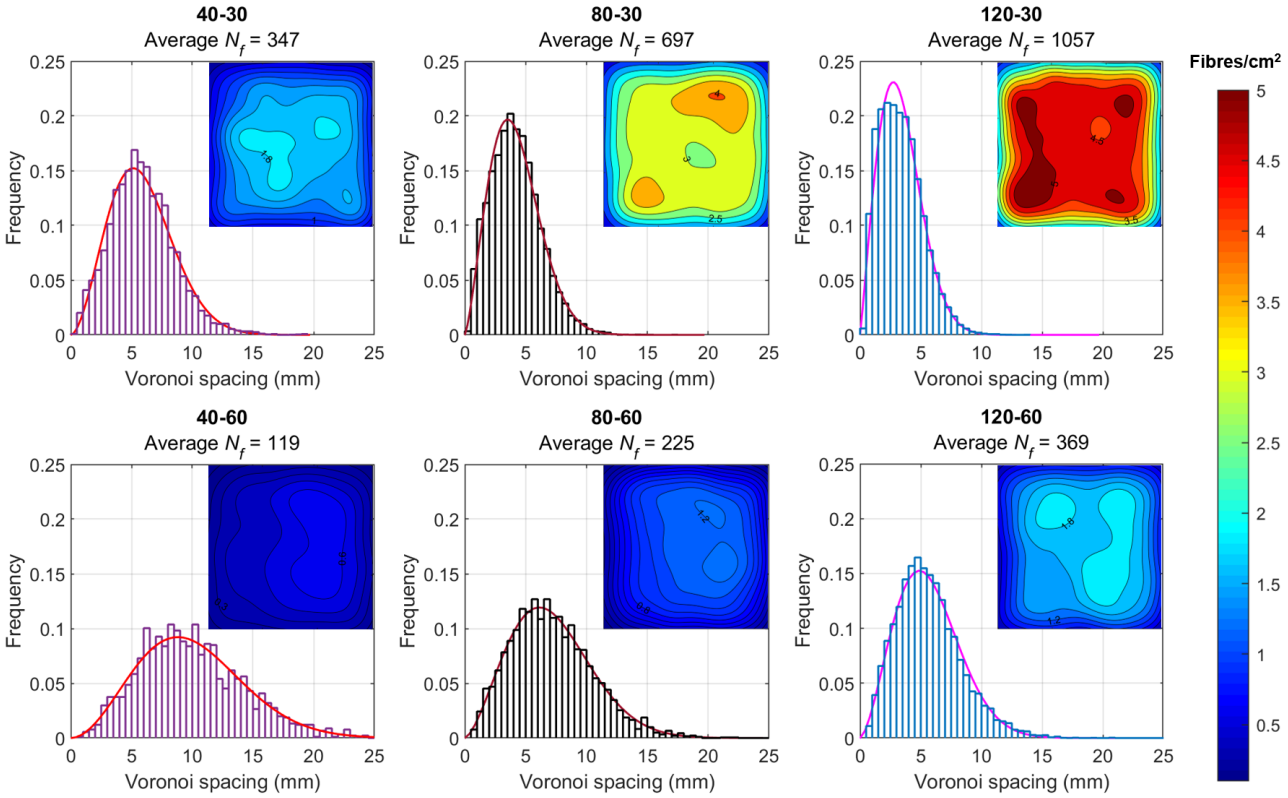

Figure 11. Histogram of Voronoi spacing results and contours of fibre density (fibres/cm^2)